# Geotechnical Aspects of Failures at Port-au-Prince Seaport during the 12 January 2010 Haiti Earthquake

**Russell A. Green,[a)] M.EERI, Scott M. Olson,[b)] M.EERI, Brady R. Cox,[c)] M.EERI, Glenn J. Rix,[d)] M.EERI, Ellen Rathje,[e)] M.EERI, Jeff Bachhuber,[f)] James French,[g)] M.EERI, Samuel Lasley,[a)] and Nathaniel Martin[b)]**

Presented herein are the results of geotechnical investigations and subsequent laboratory and data analyses of the Port-au-Prince seaport following the $M_w$7.0 2010 Haiti earthquake. The earthquake caused catastrophic ground failures in calcareous-sand artificial fills at the seaport, including liquefaction, lateral spreads, differential settlements, and collapse of the pile-supported wharf and pier. The site characterization entailed geotechnical borings, hand-auger borings, standard penetration tests, and dynamic cone penetration tests. The laboratory tests included grain size and carbonate content tests. The observations and results presented herein add valuable field performance data for calcareous sands, which are relatively lacking in liquefaction case history databases, and the overall response of the artificial fills are consistent with predictions made using semi-empirical relations developed primarily from field data of silica sands. [DOI: 10.1193/1.3636440]

## INTRODUCTION

Presented herein are the results of geotechnical field investigations, and subsequent laboratory and data analyses, for the Port International de Port-au-Prince (i.e., Port-au-Prince seaport) following the moment magnitude ($M_w$) 7.0 12 January 2010 Haiti earthquake. The port originally opened to foreign commerce in 1807 and is located slightly north of the main city center of Port-au-Prince on the Gulf of Gonâve, designated as "PaP Seaport" in Figure 1. The port facilities are primarily operated by the Autorité Portuaire Nationale (APN), although some private companies own and operate some portions of the port. The main port consists of two separate berthing and unloading facilities designated as the North Wharf and South Pier. According to data provided by APN, the port handled 978,575 metric tons of cargo in 2005 through 2006 from 490 ship calls.

[a)] Department of Civil and Environmental Engineering, 120B Patton Hall, Virginia Tech, Blacksburg, VA 24061; rugreen@vt.edu
[b)] Department of Civil and Environmental Engineering, University of Illinois at Urbana-Champaign, Urbana, IL
[c)] University of Arkansas, Department of Civil Engineering, Fayetteville, AR
[d)] School of Civil and Environmental Engineering, Georgia Institute of Technology, Atlanta, GA
[e)] Department of Civil, Architectural, and Environmental Engineering, University of Texas at Austin, Austin, TX
[f)] Fugro/William Lettis& Associates, Walnut Creek, CA
[g)] AMEC Geomatrix, Inc., Oakland, CA


*Earthquake Spectra*, Volume 27, No. S1, pages S43–S65, October 2011; © 2011, Earthquake Engineering Research Institute

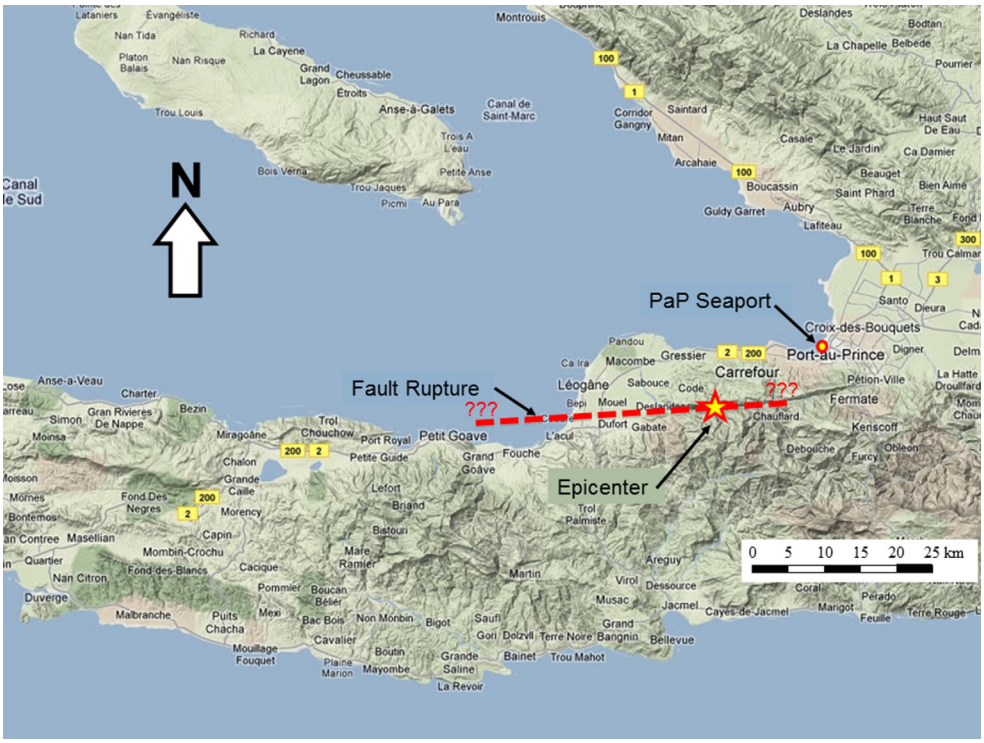


**Figure 1.** Location of the Port-au-Prince seaport and the epicenter and fault rupture of the $M_w$7.0, 12 January 2010 earthquake. Note that there is some uncertainty in the eastern and western extent of the fault rupture.

The coastlines of the port region in 1785, 1967, and 2010 are shown Figure 2, with the areas where artificial fill was placed being denoted (Ponce 1791, Army Map Service 1967, Google Earth 2010). The difference between the coastlines in 1967 and 2010 is mainly the result of fill being placed in 1976–1978 when the port was expanded. During this expansion, 28 acres of land were reclaimed from the sea. The 635,000 $m^3$ of hydraulic fill that was used to reclaim the land is composed mostly of calcareous sand and larger shell and coral fragments that were dredged from the harbor (Berniard 1978). The area in which the hydraulic fill was pumped was bounded by rock berms and a temporary dike. One to two meters of compacted gravelly fill was placed over the hydraulic fill, bringing the ground surface to its present elevation. It is unknown whether the hydraulic fill was densified, but it is doubtful given the SPT and DCPT blow counts (N-values) that were measured in the post-earthquake field investigations (discussed more in subsequent sections of this paper).

The port is approximately 18 km from the closest segment of the fault rupture of the 12 January 2010 earthquake (Figure 1; Rathje et al. 2010). The earthquake caused extensive damage to the seaport and throughout much of Port-au-Prince. Liquefaction, lateral spreading, and shaking-induced damage rendered much of the port inoperable immediately after

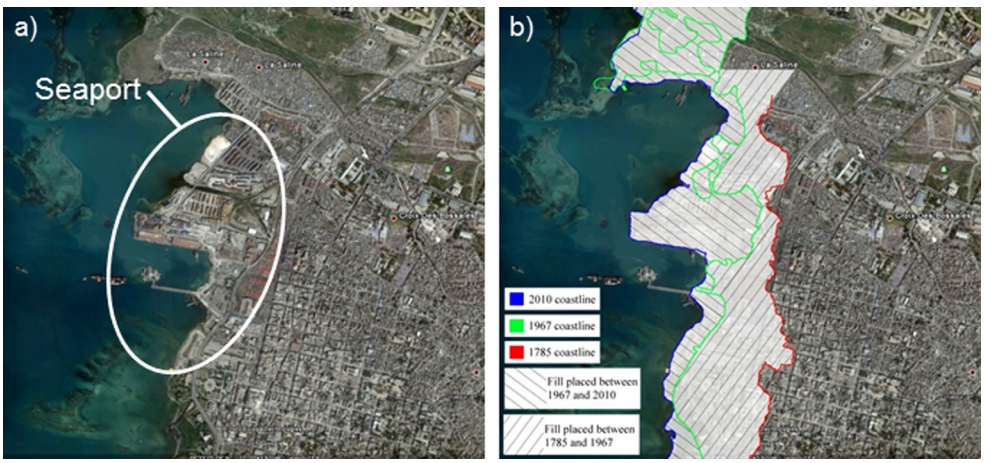


**Figure 2.** Aerial images of the seaport at Port-au-Prince: (a) Image taken shortly after the 12 January 2010 earthquake; (b) Same image shown in (a) with 1785, 1967, and present-day coastlines and artificial fill areas demarcated.

the earthquake and significantly inhibited the delivery of relief supplies to areas of Haiti affected by the earthquake.

In this paper, we detail the geotechnical damage observed at the port, focusing on the impact of liquefaction and lateral spreading; we describe *in situ* testing performed at the port as part of the post-earthquake investigations, including borehole drilling, standard penetration testing, and dynamic cone penetration testing; we analyze the triggering of liquefaction and assessment of lateral spreading using approaches available in the literature and compare those assessments to the observed performance at the port; and lastly, we discuss the relevance of our observations at the Port International de Port-au-Prince to other ports and land reclaimed with calcareous sands worldwide.

Spectral analysis of surface waves (SASW) and multi-channel analysis of surface waves (MASW) were performed as part of the post-earthquake field studies. However, the analysis and interpretation of shear wave velocity data is still ongoing and will be presented in a separate, forthcoming paper. Analyses of the structural aspects of the damage, repair methods, and post-earthquake restoration of port operations are presented in Werner et al. (2011).

## EARTHQUAKE-INDUCED GEOTECHNICAL DAMAGE AT THE PORT INTERNATIONAL DE PORT-AU-PRINCE

Pre- and post-earthquake aerial images of the port are shown in Figure 3. Light-colored areas on the ground surface in Figure 3b are sand boils and ejecta that were observed in the eastern half of the container storage yard and behind and between the two warehouses. The locations where large lateral spreading fissures were observed are also shown in Figure 3b. These images clearly show evidence of liquefaction and lateral spreading, collapse of the North Wharf, and collapse of portions of the South Pier. Damage to the South Pier is detailed in Werner et al. (2011) and is not discussed in detail in this paper.


(a)

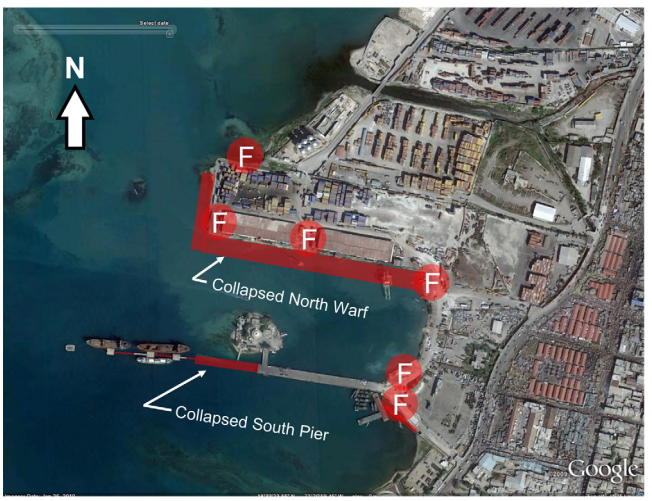


(b)

**Figure 3.** Aerial images of seaport at Port-au-Prince, (a) prior to earthquake; and (b) after the earthquake illustrating ground failures, marked with "F," and damage to South Pier and North Wharf.

## DAMAGE TO THE NORTH WHARF

The North Wharf was a 450-m long by 21-m wide, pile-supported marginal wharf constructed in 1976–78 by a U.S. contractor (Berniard 1978). The water depth adjacent to the wharf is 8 to 10 m. The wharf deck was supported by 72 pile bents spaced 6.7 m on center;

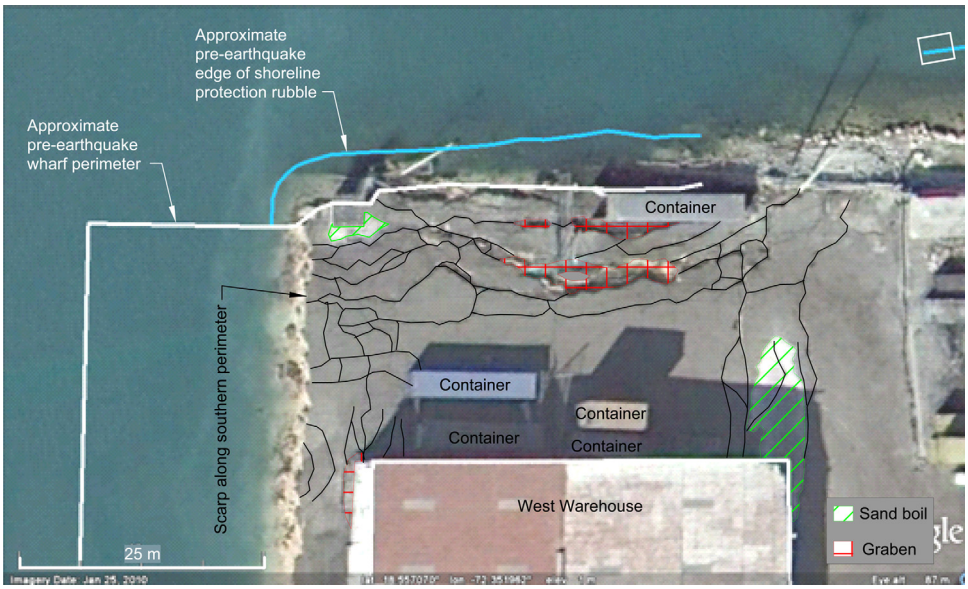


**Figure 4.** Aerial view and schematic of ground failure at western end of North Wharf. Pre-earthquake image dated 26 August 2009 used for pre-failure perimeter. Post-failure image taken on 13 January 2010. Manual survey performed on 1 February 2010. Warehouse width is approximately 37 m, with an additional 4 m overhanging roof on the north side of structure.

each bent had five rows of vertical piles and one row of opposing batter piles. All the piles were 45.7 cm × 45.7 cm square precast, prestressed concrete piles between 25 and 29 m in length and were cast in Haiti in a yard setup by the U.S. contractor that built the wharf. Construction drawings and photos indicate that the piles were driven first, with fill for an embankment placed subsequently using a clamshell. An inspection of the wharf conducted in 2007 found evidence of significant deterioration. Of the 72 bents, 38 (53%) had occurrences of "cracks greater than 5 mm in width" and/or "visible steel and/or missing concrete." Fifty-eight (12%) of the 504 piles had similar defects or were "destroyed."

Immediately adjacent to the wharf are two steel-frame warehouses, each approximately 150 m by 40 m. A storage yard is located immediately north of the warehouses, and a large number of mostly empty containers stacked two- to four-high were present in the storage yard at the time of the earthquake. There were three cranes at the North Wharf at the time of the earthquake, including one 15-m gauge A-frame container crane and two rubber-tired mobile cranes.

The North Wharf suffered extensive liquefaction, evidenced by the ejecta present along the wharf, and lateral spreading along its southern, western, and northern perimeters. Along the southern perimeter, we measured a cumulative maximum horizontal movement of 89 cm (determined by crack widths) in a zone extending inland approximately 30 m from the post-earthquake shoreline. However, imagery taken shortly after the earthquake indicates

**Figure 5.** Submerged 15-m gauge container crane (foreground) and mobile crane (background).

that lateral spread cracking extended 50 m inland from the damaged edge of the wharf, but most of these inland lateral spread cracks were covered with fill soon after the earthquake so that vehicle traffic could pass. Furthermore, comparison of pre- and post-earthquake aerial imagery indicates that the concrete marginal wharf and adjacent fill moved laterally 15 m or more south and into the bay.

Figure 4 presents a schematic of the lateral spread that occurred along the western perimeter of the North Wharf's fill embankment. We measured a cumulative total of 2.6 m of lateral displacement, but this magnitude likely underestimates the actual maximum displacements at the original western edge of the wharf, as some of the displaced portion of the embankment flowed into the bay and was not accessible. Moderate lateral spreading also occurred along the northern perimeter of the wharf but was not measured.

The A-frame container crane and one rubber-tired crane displaced into the bay along with the concrete marginal wharf, rendering them inoperable, but they appeared to be undamaged. The second mobile crane was parked between the two warehouses and was undamaged. Figure 5 shows the A-frame container crane in the foreground and the partially submerged rubber-tired mobile crane in the background. Interestingly, a photo taken immediately after the earthquake from aboard a ship docked at the eastern end of the wharf (Figure 6) shows that the landside legs of the A-frame crane were still above water and near the easternmost end of its tracks, although the tracks had moved seaward about 2 m relative to the adjacent land. However, a U.S. Coast Guard photo taken during an over flight of the port at midday on 13 January 2010 shows the crane in the same position as in Figure 5 (i.e., moved westward about 50m west and about 15 m south from its position in Figure 6) and with the base of the crane fully submerged. The 13 January

**Figure 6.** Photo taken immediately after the earthquake with the crane in its most eastward position and with the landside legs of the crane above water. Photo taken facing east. (gCaptain, 2010).

2010 photo also shows that additional subsidence occurred at the eastern end of North Wharf (i.e., the location of the crane in Figure 6). The National Earthquake Information Center reported that no fewer than 45 aftershocks ranging from $M_w$ 4.0 to 6.0 occurred between the main shock and 1:54 pm EST on 13 January 2010 (Rathje et al. 2010). This suggests that a portion of the observed permanent displacements may have been caused by liquefaction that occurred as a result of aftershocks.

Significant damage to the steel warehouses along the southern half of the north wharf also occurred. As shown in Figure 7, lateral spreading cracks running in the east-west direction cut through each of the warehouses' foundation walls. A detailed survey of the settlements relative to the north edge of the western-most bay and lateral movements of the west warehouse slab are shown in Figure 8. The interior slab consisted of 14 separate slabs, two each in seven bays. Due to lateral spreading, the south wall (adjacent to the shoreline) moved approximately 0.7 to 1.4 m laterally towards the shoreline (i.e., the width of the warehouses increased). The settlements across the warehouse interior were variable, with the southern sections settling as much as ~0.8 m. It appeared that the warehouses were founded on strip footings around their perimeters, which settled significantly. Settlements measured at the adjacent inland corners of the warehouses were about 15 cm at the west warehouse (see Figure 8) and more than 40 cm at the east warehouse.

**Figure 7.** Lateral spreading crack extending into the western foundation wall of the west warehouse.

## GEOTECHNICAL DAMAGE TO OTHER PORT FACILITIES

North of the main port facility along the shoreline, there were six steel grain hopper silos and two storage yards (Figure 9). Construction of the grain silos started in July 2009 and was mostly completed at the time of the earthquake, with only the grain conveyor systems still needing to be installed according to onsite facility personnel. Consequently, the

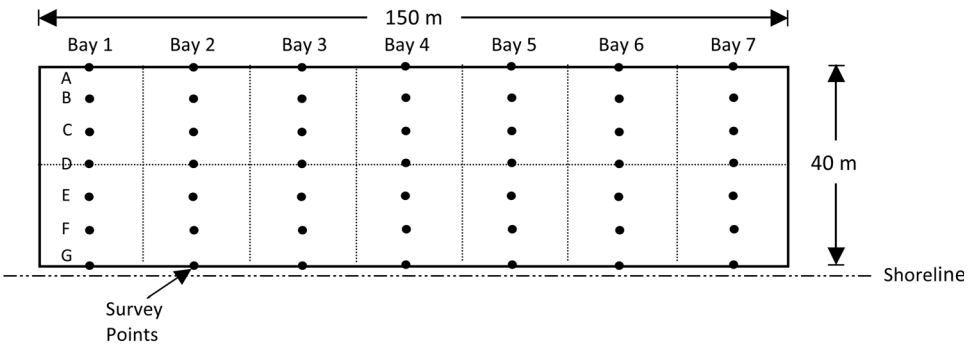


| | Survey Pt | Bay 1 | Bay 2 | Bay 3 | Bay 4 | Bay 5 | Bay 6 | Bay 7 |
|---|---|---|---|---|---|---|---|---|
| Vertical Settlement (cm) | A | 0.0 | -6.1 | 27.5 | 42.7 | -7.6 | 32.0 | -4.6 |
| | B | -7.3 | -4.3 | -2.7 | 24.7 | -14.9 | 24.7 | -5.8 |
| | C | -20.4 | -20.4 | -25.0 | -32.6 | -23.5 | -43.3 | -0.6 |
| | D | -24.4 | -18.3 | -21.4 | -2.7 | -13.7 | -47.3 | 0.0 |
| | E | -6.7 | -32.6 | -8.2 | -11.3 | -5.2 | -23.5 | -15.9 |
| | F | -16.5 | -25.6 | -25.6 | -34.8 | -19.5 | -27.1 | -25.3 |
| | G | -48.8 | -63.4 | -74.7 | -79.3 | -67.1 | ? | -58.0 |

| | | | | | | | |
|---|---|---|---|---|---|---|---|
| Displacement of south wall towards south (cm) | 71.1 | 94.9 | 119.9 | 104.6 | 141.5 | 131.8 | 84.8 |

** Assumed datum at north edge of Bay 1. All data based on survey with hand level with values adjusted to correct for apparent instrument bias*

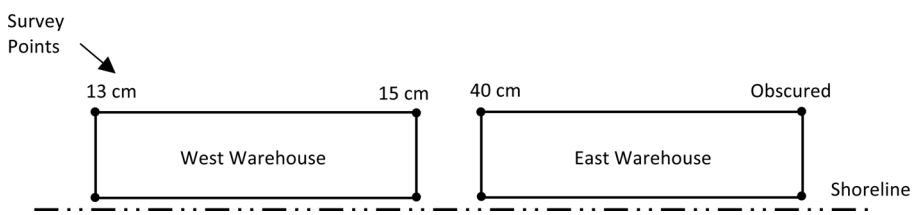


**Figure 8.** Results of a detailed survey of the relative settlement of the west warehouse slab and total settlement of inland corners and total lateral displacement of seaward side of west warehouse. All displacements inside warehouse measured relative to survey location in northwest corner of warehouse. Displacements at NW and NE warehouse corners indicate relative settlement of ground surface with respect to warehouse wall. Displacements along southern warehouse wall indicate lateral movement of wall with respect to floor slab.

silos were empty at the time of the earthquake. The silos were manufactured by SCAFCO Grain Systems Company, with each having an overall height of about 26.1 m and weight of about 420 kN. SCAFCO recommends two differently-dimensioned shallow foundations for this model silo, one accounting for overturning moments due to seismic loading (UBC Seismic Zone 3) and wind loading and the other not. Both are ring footings and have embedment depths of approximately 1.14 m. The foundation design that accounts for overturning due to seismic and wind loading is more heavily reinforced, has an ~8.14 m outside radius,


(a) (b)

**Figure 9.** Steel grain silos north of the main seaport: (a) Photograph taken from the ground facing northeast; (b) aerial image of silos taken after the earthquake with lateral spread cracks demarcated.

and has an ~5.18 m width, while the other is more lightly reinforced, has an ~7.26 m outside radius, and has an ~2.44 m width. It is unknown which of these foundations was used, if either. However, surficial cracks in the soil around the base of the silos (Figure 10) suggest that the silos have shallow ring footings with an outside radius of ~7.26 m, with the cracks in the soil resulting from footing uplift caused by seismically induced overturning moments. If this is indeed the case, our preliminary calculations indicated that the silos likely would have overturned if they had been filled with grain at the time of the earthquake.

A unique aspect of the silos is that they were built on a garbage fill overlain by compacted gravel/cobbles (Rathje et al. 2010). Based on the depth of lateral spread cracks in the fill adjacent to the silos (Figure 9b), it is estimated that the garbage fill is at least 2 m thick. The cumulative lateral spreading displacement in the fill adjacent to the silos was

**Figure 10.** Crack in the soil around the base of the silos. This crack was likely made from uplift of the footing due to overturning moments induced by the earthquake shaking.

**Figure 11.** Lateral spreading in the storage yards in the northern part of the port facility.

about 1.2 m. However, detailed inspection of the sidewalls of the lateral spreading-induced cracks showed that the garbage fill experienced almost no lateral distortion (i.e., the walls of the lateral spreading cracks were nearly vertical). Accordingly, the authors believe that lateral spreading was caused by liquefaction of sand underlying the garbage fill and that slabs of the garbage fill moved laterally and monolithically on top of the liquefied sand.

Extensive lateral spreading also occurred in two storage yards located just north of the silos (Figure 11). Approximately 2.4 m of cumulative lateral displacement was measured at the northern storage yard. Similar to the silo area, these storage yards were constructed on garbage fill overlain by compacted gravel/cobbles (Rathje et al. 2010). Based on detailed inspection of the sidewalls of the lateral spreading cracks, the authors believe that lateral spreading was caused by liquefaction of sand underlying the garbage fill, similar to the lateral spreads that occurred adjacent to the silos.

A bridge connecting the silo area to the storage yards performed reasonably well during the earthquake, suffering only minor damage. The bridge is a three-span, bulb-T concrete beam bridge with each of the two intermediate piers and the abutments founded on four ~41-cmsquare precast concrete piles (Figure 12). As may be observed in Figure 13, minor crushing occurred between the northern and middle spans. Also, transverse movement (~10 cm) occurred between the southern and middle spans (see Figure 13). The south abutment fill soils showed negligible movements toward the drainage canal, while the north abutment fills slumped approximately 15 cm on the western side and approximately 5 cm on the eastern side. Several ground cracks also formed in the abutment fill cone near the waterline in the canal.


**Figure 12.** Profile of bridge connecting silo area to northernmost storage yards. Photograph taken looking eastward (i.e., the north end of the bridge is to the left).

Finally, one of the main entrance roads to the port was heavily damaged by liquefaction-induced lateral spreading, exhibiting on the order of 1 m of lateral and vertical movements.

## SUBSURFACE CONDITIONS AT THE PORT-AU-PRINCE SEAPORT

Post-earthquake subsurface investigations at the port included borehole drilling and sampling, standard penetration tests (SPT), and dynamic cone penetration tests (DCPT). Figure 14 presents the locations of the tests performed at the port.

**Figure 13.** Minor crushing and lateral offset of middle and southern bridge spans for bridge connecting silo area to northernmost storage yards. Photograph taken looking northward.


**Figure 14.** Location of borings with standard penetration tests and dynamic cone penetration tests.

Drilling was performed by Horizon Consultants (Santo Domingo, Dominican Republic) using a CME 55 drill rig with an automatic hammer system, A-sized rods, and hollow-stem augers. The energy ratio for the SPT hammer system was measured in accordance with ASTM D4633-10 and found to have a mean value of 85% (i.e., about 25% more than the standard 60% for a rope and cathead). The split spoon was designed for a liner, but no liners were used in the testing performed for this study. Although mud rotary drilling is preferred to hollow-stem augers for liquefaction field studies (e.g., Seed et al. 1984), we used the best available equipment that was able (and willing) to be transported to Haiti.

The dynamic cone penetrometer used for this study was originally designed by Professor George Sowers (Sowers and Hedges 1966) and built by Humboldt Manufacturing Co. The DCPT is highly portable and suitable for immediate post-earthquake reconnaissance investigations. This system utilizes a 6.8 kg mass (15-lb drop weight) on an E-rod slide drive to penetrate an oversized 45° apex angle cone. The cone is oversized to reduce rod

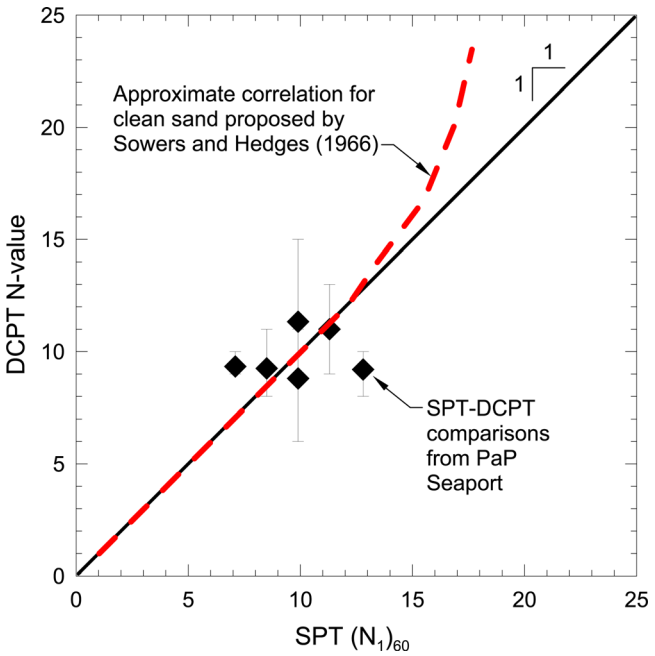


**Figure 15.** Comparison of SPT $(N_1)_{60}$ values and DCPT N-values measured at PaP Seaport.

friction behind the tip. Hand-auger holes were drilled in conjunction with the DCPT to determine stratigraphy (to depths slightly below the groundwater table), to minimize rod friction, and to collect soil samples.

Although a DCPT-based liquefaction evaluation procedure does not exist, a comparison of DCPT penetration resistance with SPT blow count suggests that a 1:1 correlation provides a reasonable match between the two data sets (Figure 15). This 1:1 correlation is consistent with the correlation for sands (with SPT blow count less than about 15) recommended by Sowers and Hedges (1966). As a result, we assumed a 1:1 correlation for all subsequent subsurface characterization and liquefaction analyses. Finally, the DCPT has been used on several other recent post-earthquake investigations (e.g., 2010, $M_w$ 8.8 Maule, Chile, earthquake and the 2010, $M_w$7.1 Darfield, New Zealand, earthquake) to evaluate deposits that liquefied.

Using the hand-auger logs, boring logs, and subsurface samples retrieved from the site, the authors developed subsurface profiles at the south end of the north wharf. The profile is presented in Figure 16. Figure 17 presents additional DCPT and SPT data.

Figure 18 presents grain size distributions of sands retrieved from hand-augered boreholes for soundings DCPT-5 and 6, and illustrate the well-graded nature of the fill sands at the site. The coarser fraction of the samples consists of subrounded to subangular sands and gravels, with large fragments of coral and shells causing the grain size distribution to

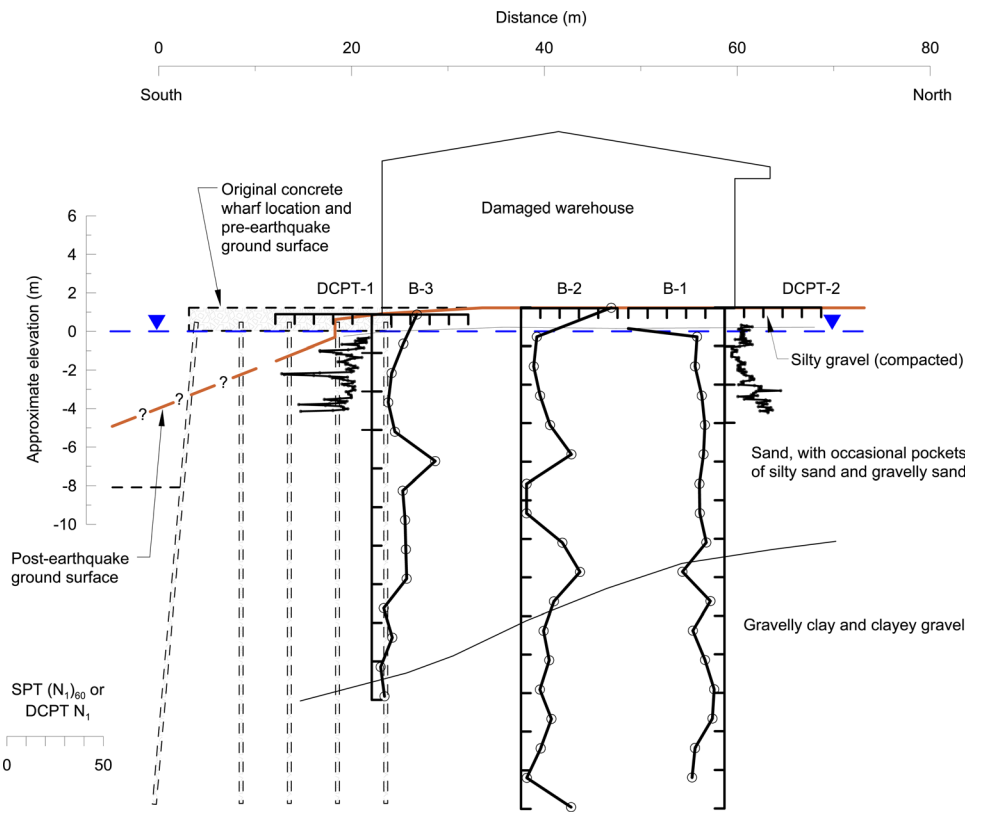


**Figure 16.** Geotechnical profile of south edge of North Wharf.

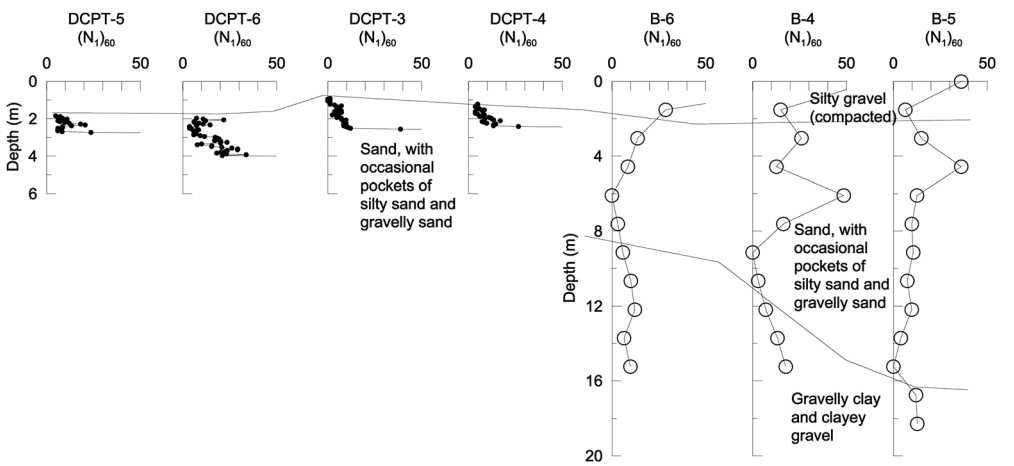


**Figure 17.** Additional penetration test results from North Wharf and South Pier areas.

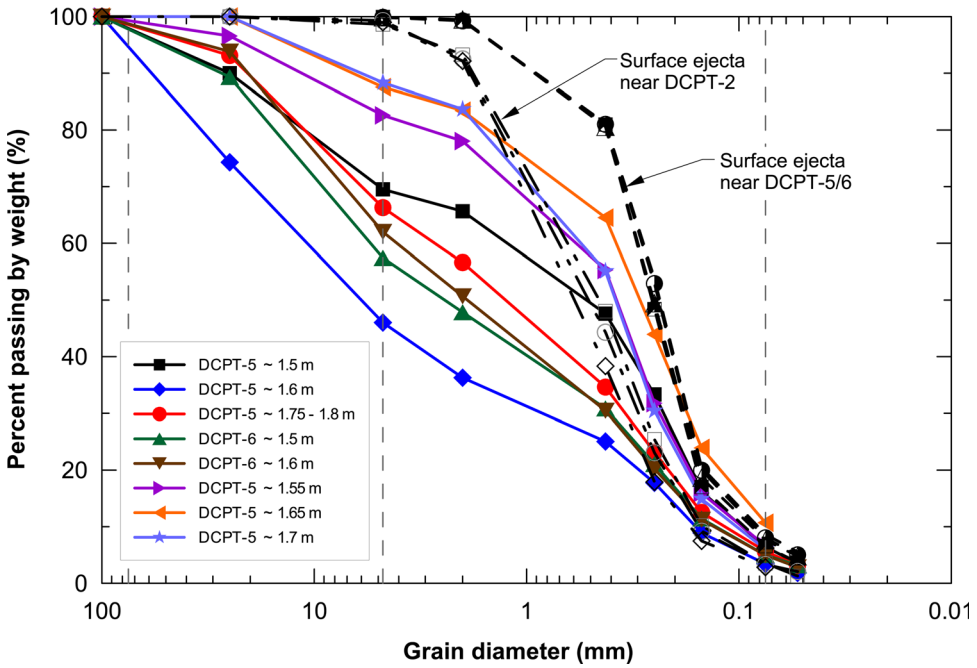


**Figure 18.** Grain size distributions for samples obtained from hand augered borehole adjacent to soundings DCPT-5 and DCPT-6, and grain size distributions for sand boil ejecta samples obtained near DCPT-5/6 and DCPT-2.

appear broader than the calcareous matrix sand. This is also evidenced by the grain size distributions of the ejecta retrieved from the surface sand boils observed near DCPT-2 and DCPT-5/6, which show almost no gravel-sized particles. Both the *in situ* samples and surface ejecta samples were relatively clean sands, with most samples exhibiting a fines content (FC) less than 5%, and all samples exhibiting FC < 8%. The fines are calcareous and generally nonplastic when considered as a mass, although the fines fraction contained a small amount of low plasticity material based on the moderate dry strength of a thin crust that formed on the ejecta.

Additionally, gasometric carbonate content tests (calcite equivalent) were performed on samples from some of the hand-augered boreholes and ejecta. The tests were performed in general accordance with ASTM D4373-02 (ASTM, 2010). The samples were allowed to react with the hydrochloric acid (HCl) for 10 minutes, with carbon dioxide ($CO_2$) gas pressure readings taken periodically. The tests were stopped after 10 minutes because the gas pressure in the reactor stabilized, indicating that the HCl-carbonate reaction was complete. For the tested samples, the equivalent calcite content ($CaCO_3$) ranged from 85 to 89%, which is consistent with soils comprised of coral sands, shell fragments, and sand derived from nearby weathered limestone.

**Table 1.** Source, distance, and site response parameters for the NGA ground motion predition models (Wells 2010)

| | | |
|---|---|---|
| Source Parameters | Moment Magnitude: $M_w$ | 7.0 |
| | Depth to top of rupture: $Z_{TOR}$ | 2 km |
| | Fault type | reverse oblique |
| | Dip angle: $\delta$ | 55° |
| | Down-dip rupture width: W | 22 km |
| Distance Parameters | Closest distance to rupture surface: $R_{rup}$ | 18 km |
| | Closest distance to the surface projection of the fault rupture: $R_{jb}$ | 18 km |
| | Horizontal distance from the top edge of the rupture, measured perpendicular to the fault strike: $R_x$ | 18 km |
| Site Response Parameters | $V_{s,30m}$ | 350 m/s |
| | Depth to the 1 km/s shear wave velocity horizon: $Z_{1.0}$ | 346 m |
| | Depth to the 2.5 km/s shear wave velocity horizon: $Z_{2.5}$ | 1.764 km |

## INTERPRETATION OF CYCLIC LIQUEFACTION BEHAVIOR

Widespread liquefaction occurred at the port as a result of the earthquake. The availability of SPT and DCPT at the port provides a unique opportunity to assess liquefaction and lateral spreading using two different, yet related, *in situ* testing results.

### ESTIMATE OF GROUND SHAKING AT SEAPORT

Regrettably, no strong motion instruments were operating in Haiti at the time of the earthquake to record the ground motions during the 12 January 2010 event. Therefore, the geometric mean of the peak ground accelerations (PGA) predicted by four of the Next Generation Attenuation (NGA) ground motion prediction relationships (Abrahamson and Silva, 2008; Boore and Atkinson, 2008; Campbell and Bozorgnia, 2008; Chiou and Youngs, 2008) were used to estimate the PGA at the port. The input parameters used to predict the PGA are listed in Table 1 (Wells, 2010). The resulting PGA is approximately $0.22g \pm 0.12g$.

### LEVEL-GROUND LIQUEFACTION ANALYSIS

Liquefaction analysis for level-ground conditions is commonly performed using the "simplified" liquefaction evaluation procedure pioneered by Whitman (1971) and Seed and Idriss (1971). More recently, this approach has been updated by Youd et al. (2001), Cetin et al. (2004), and Idriss and Boulanger (2008). As the Youd et al. (2001) approach has been thoroughly vetted, we opted to use this procedure (i.e., the magnitude scaling factor, depth reduction factor, overburden stress correction, etc.) to assess liquefaction at the seaport using SPT and DCPT results.

Figure 19 and Table 2 present the liquefaction analysis using SPT borings B-1 through B-6, as well as DCPT soundings 1 through 6. Although neither the SPT N-values (performed through hollow-stem augers) nor DCPT N-values are preferred for evaluating

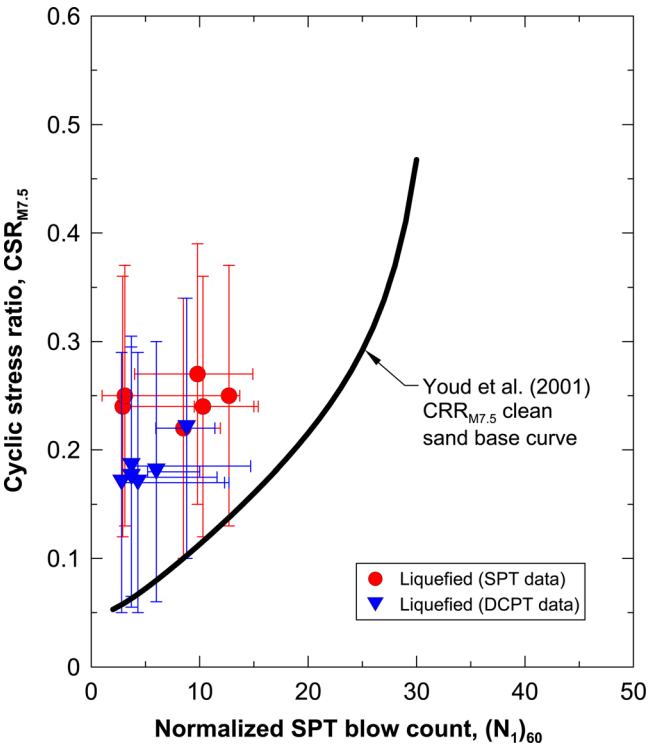


**Figure 19.** Level ground liquefaction analysis for SPT and DCPT results, to include error bars. Note that CRR base curve was derived from mathematical expression in Youd et al. (2001).

liquefaction potential, these computations clearly illustrate that the seaport fills are highly susceptible to liquefaction. Additionally, the SPT N-values suggest that the sands may be very loose to depths ranging from 5 to 19 m, consistent with the severe liquefaction effects observed at the surface.

## LIQUEFACTION-INDUCED LATERAL SPREADING ANALYSIS

Lateral spreads are complex dynamic problems involving liquefaction triggering, estimating lateral displacements, and evaluating soil-foundation interaction. Many studies are available to evaluate triggering of lateral spreads and the resulting displacements, including empirical techniques (e.g., Rauch and Martin 2000, Youd et al. 2002), laboratory studies (e.g., Zhang et al. 2004, Idriss and Boulanger 2008), centrifuge studies (e.g., Taboada-Urtuzuastegui and Dobry 1998, Kutter et al. 2004), and numerical techniques (e.g., Chiru-Danzer et al. 2001, Baziar and Ghorbani 2005).

The magnitudes of the lateral spreads at the seaport are difficult to quantify, but the large lateral spread at the south end of the North Wharf was well-documented in terms of *in situ* testing, providing an opportunity to test multiple empirical and laboratory-based

**Table 2.** Summary of SPT and DCPT data at Port-au-Prince seaport during 2010 Haiti earthquake

| Test ID | Critical depth* (m) | Water depth (m) | N-value | $C_N$ | $(N_1)_{60}$-value | Fines content (%) | Median grain diameter (mm) | $r_d$ | Equivalent CSR for M = 7.5 and median pga |
|---|---|---|---|---|---|---|---|---|---|
| B-1 | 6.1 | 1.5 | 6 | 1.27 | 10.3 | 4 | ~ 0.5 (sand) | 0.96 | 0.24 |
| B-2 | 9.1 | 1.8 | 2 | 1.06 | 2.9 | ~ 5 | ~ 0.5 (sand) | 0.92 | 0.24 |
| B-3 | 4.6 | 1.5 | 5 | 1.41 | 8.5 | ~ 5 | ~ 0.5 (sand) | 0.97 | 0.22 |
| B-4 | 4.6 | 0.9 | 7 | 1.5 | 12.7 | ~ 5 | ~ 0.5 (sand) | 0.97 | 0.25 |
| B-5 | 7.6 | 0.9 | 6 | 1.21 | 9.8 | ~ 5 | ~ 0.5 (sand) | 0.94 | 0.27 |
| B-6 | 7.6 | 1.5 | 2 | 1.16 | 3.1 | ~ 5 | ~ 0.5 (sand) | 0.94 | 0.25 |
| DCPT-1 | 3.8 | 1.3 | 8 | 1.54 | 8.8 | ~ 5 | ~ 0.5 (sand) | 0.97 | 0.22 |
| DCPT-2 | 2.4 | 1.5 | 3 | 1.70 | 3.6 | 4 | ~ 0.45 (sand) | 0.98 | 0.18 |
| DCPT-3 | 1.8 | 1.2 | 2 | 1.70 | 2.4 | ~ 5 | ~ 0.5 (sand) | 0.99 | 0.17 |
| DCPT-4 | 1.7 | 1.2 | 3 | 1.70 | 3.6 | ~ 5 | ~ 0.5 (sand) | 0.99 | 0.17 |
| DCPT-5 | 2.5 | 1.5 | 5 | 1.70 | 6.0 | 5 | ~ 1(0.25 sand) | 0.98 | 0.18 |
| DCPT-6 | 2.5 | 1.5 | 3 | 1.70 | 3.6 | 5 | ~ 1(0.25 sand) | 0.98 | 0.18 |

*Critial depth corresponds to the depth of liquefaction.

methods. The depth of the water near the North Wharf was approximately 10 m. Table 3 compares the measured/estimated lateral displacement to the predicted displacements. As illustrated in the table, predictive methods appear to underestimate the displacements experienced at the south end of the North Wharf. However, all of the empirical and laboratory-based methods predicted large, destructive lateral displacements that would require mitigation in engineering design.

## RELEVANCE TO OTHER PORTS AND AREAS OF RECLAIMED LAND

The data presented herein adds to the limited number of documented case histories where calcareous sands liquefied/laterally spread during earthquakes. Other documented

**Table 3.** Comparison of measured/estimated and predicted displacements at south edge of North Wharf

| Method | Lateral Displacement (m) |
|---|---|
| Measured/estimated | >> 0.9 (likely ~ $15^+$ after aftershocks) |
| Youd et al. (2002) | 1.7 (range ~ 1.0 – 1.8) |
| Rauch & Martin (2000) | 1.7 (range ~ 1.6 – 1.7) |
| Zhang et al. (2004) | ~ 1.5 to ~ 6[(1)] |
| Idriss & Boulanger (2008) | ~ 1.5 to ~ 6[(1)] |

[(1)]Smaller value computed from DCPT results, larger value computed from SPT results

cases of liquefaction and lateral spreading failures of calcareous sands at port facilities include the 1993, $M_w$7.7 Guam earthquake (Mejia and Yeung 1995), and Kawaihae Harbor during the 2006, $M_w$6.7 and $M_w$6.0 Hawaii earthquakes (Brandes et al. 2007). Similar to the PaP seaport in Haiti, the simplified liquefaction evaluation procedure predicted that the calcareous sand deposits at these sites would liquefy, when best estimates of the induced cyclic stress ratios and measured penetration resistances were used. This is significant because the semi-empirical SPT-based liquefaction evaluation procedure is based almost solely on case histories involving silica sand, not calcareous sand. Also, past studies have shown conflicting results when penetration resistance-based techniques and shear wave velocity-based techniques have been used to evaluate liquefaction potential at the same sites (e.g., Nicholson, 2006). Furthermore, cone penetration tests-based techniques were used to evaluate liquefaction potential at the Palm Islands in Dubai, which were reclaimed using calcareous sand. Concerns for liquefaction at the site resulted in one of the largest vibrocompaction projects ever undertaken (Gunberg et al. 2007).

## SUMMARY AND CONCLUSIONS

The $M_w$7.0, 12 January 2010 Haiti earthquake caused extensive damage to the Port International de Port-au-Prince. During three separate reconnaissance missions, the authors documented the geotechnical failures and performed geotechnical site characterization that included geotechnical borings, hand auger borings, standard penetration tests, dynamic cone penetration tests, and laboratory index testing.

Lateral spreading at the North Wharf destroyed the southern, western, and northern perimeter, with observed lateral displacements likely 15 m or more, over 2.6 m, and $\sim$1 m, respectively. Approximately 1.2 m of cumulative lateral spreading displacement occurred at a grain silo yard north of the North Wharf, and approximately 2.4 m of lateral spreading displacement occurred at a storage yard north of the grain silo area.

The grain silos appeared to have suffered little structural damage as a result of the earthquake shaking. However, surficial cracks in the soil around the base of the silos suggest that uplifting of shallow ring footing occurred due to seismically induced overturning moments. Preliminary calculations performed by the authors suggests that the silos would likely have overturned if they had been filled with grain at the time of the earthquake.

Using the *in situ* testing results, we describe 12 new liquefaction case records involving relatively clean, calcareous sands (Figure 18 and Table 2), which are not well documented in the literature. In addition, we compare measured/estimated lateral spreading displacements to the displacements predicted by often-employed empirical and laboratory-based procedures. Although the field-observed liquefaction and lateral spread responses of these calcareous sands were compared with semi-empirical procedures that were developed primarily using field data of silica sands, the overall response of the artificial fills are reasonably consistent with predictions.

The results obtained at the seaport at Port-au-Prince are particularly valuable because similar seismic behavior may be expected at many sea and river ports and other areas of reclaimed land around the world that involve hydraulically-placed calcareous sands.

## ACKNOWLEDGEMENTS

This material is based on work supported by the National Science Foundation under Grant No. CMMI-1025582 and CMMI-1034793. Any opinions, findings, and conclusions or recommendations expressed in this material are those of the authors and do not necessarily reflect the views of the National Science Foundation. The authors acknowledge Dr. Frank Rausche of GRL Engineers, Inc. and Pile Dynamics, Inc. for providing the equipment used for SPT energy measurements, Mr. Alan Crumley and Mr. Ricardo Fabré of GeoConsult for providing valuable assistance with planning and coordinating the soil borings, Mr. Daniel Wambeke of SCAFCO Grain Systems Co. for providing information about the grain silos, and Mr. Donald Wells of AMEC Geomatrix, Inc. for providing the source and input parameters for the NGA ground motion prediction relationships.

## REFERENCES

Abrahamson, N., and Silva, W., 2008. Summary of the Abrahamson & Silva NGA ground-motion relations, *Earthquake Spectra* **24**, 67–97.

Army Map Service, 1967. *Port-au-Prince and Vicinity 1:12,500 scale map*, Army Map Service (SX), Corps of Engineers, U.S. Army, Washington, D.C.

ASTM International (ASTM D4373-02), 2010. *Standard Test Method for Rapid Determination of Carbonate Content of Soils*, D4373-02 (Reapproved 2007), ASTM International, West Conshohocken, PA.

ASTM International (ASTM D4633-10), 2010. Standard Test Method for Energy Measurement for Dynamic Penetrometers, D4633-10, ASTM International, West Conshohocken, PA.

Berniard, S., 1978. Raymond International working on $20 million Haiti port project, *Florida Builder*, 3–9.

Baziar, M. H., and Ghorbani, A., 2005. Evaluation of lateral spreading using artificial neural networks, *Soil Dynamics and Earthquake Engineering* **25**, 1–9.

Boore, D. M., and Atkinson, G. M., 2008. Ground-motion prediction equations for the average horizontal component of PGA, PGV, and 5%-damped PSA at spectral periods between 0.01 s and 10.0 s, *Earthquake Spectra* **24**, 99–138.

Brandes, H. G., Nicholson, P. G., and Robertson, I. N., 2007. Liquefaction of Kawaihae Harbor and Other Effects of the 2006 Hawai'i Earthquakes, *Proc. of the 7th Intern. Offshore and Polar Conf.*, ISOPE, 1169–1176.

Campbell, K. W., and Bozorgnia, Y., 2008. NGA ground motion model for the geometric mean horizontal component of PGA, PGV, PGD and 5% damped linear elastic response spectra for periods ranging from 0.01 to 10 s, *Earthquake Spectra* **24**, 139–171.

Cetin, K. O., Seed, R. B., Der Kiureghian, A., Tokimatsu, K., Harder, L. F., Jr., Kayen, R. E., and Moss, R. E. S., 2004. Standard penetration test-based probabilistic and deterministic assessment of seismic soil liquefaction potential. *Journal of Geotechnical and Geoenvironmental Engineering*, ASCE, **130**, 1314–1340.

Chiou, B. S.-J., and Youngs, R. R., 2008. An NGA Model for the Average Horizontal Component of Peak Ground Motion and Response Spectra, *Earthquake Spectra* **24**, 173–215.

Chiru-Danzer, M., Juang, C. H., Christopher, R. A., and Suber, J., 2001. Estimation of liquefaction-induced horizontal displacements using artificial neural networks. *Canadian Geotechnical Journal* **38**, 200–207.

gCaptain, 2010. http://gcaptain.com/maritime/blog/port-prince-earthquake-damage/

Google Earth, 2010.

Gunberg, K. A., Green, R. A., and Ashmawy, A. K., 2008. The time-dependent changes in the state and properties of the recently deposited palm island sands in Dubai, *Proc. International Research and Education in Engineering Conference*, West Lafayette, IN, October 30–November 1, 2007.

Idriss, I. M., and Boulanger, R. W., 2008. *Soil Liquefaction during Earthquakes*, EERI Monograph MNO-12, Earthquake Engineering Research Institute, 237 pp.

Kutter, B. L., Gajan, S., Manda, K. K., Balakrishnan, A., 2004. Effects of layer thickness and density on settlement and lateral spreading, *Journal of Geotechnical and Geoenvironmental Engineering*, ASCE, **130**, 603–614.

Mejia, L. H., and Yeung, M. R., 1995. Liquefaction of coralline soils during the 1993 Guam earthquake, *Earthquake-Induced Movements and Seismic Remediation of Existing Foundations and Abutments* (S. Kramer and R. Siddharthan, eds.), Geotechnical Special Publication No. 55, ASCE, 33–48.

Ponce, N., 1791. Plan de la Ville des Rades et des Environs du Port-au-princedansl'isle Saint Domingue, Recueil de vues des lieuxprincipaux de la coloniefrançoise de Saint-Domingue, Paris, obtained from the John Carter Brown Library, Brown University (JCB Call Number E791 P793r/3-SIZE).

Rathje, E., Bachhuber, J., Cox, B., French, J., Green, R. A., Olson, S., Rix, G., Wells, D., and Suncar, O., 2010. *Geotechnical Engineering Reconnaissance of the 2010 Haiti Earthquake*, GEER Association Report No. GEER-021, http://www.geerassociation.org/GEER_Post%20EQ%20Reports/Haiti_2010/Cover_Haiti10.html.

Rauch, A. F., and Martin, J. R., II., 2000. EPOLLS model for predicting average displacements on lateral spreads, *Journal of Geotechnical and Geoenvironmental Engineering*, ASCE, **126**, 360–371.

Seed, H. B., and Idriss, I. M., 1971. Simplified procedure for evaluating liquefaction potential, *Journal of the Soil Mechanics and Foundations Division*, ASCE, **97**, 1249–1273.

Seed, H. B., Tokimatsu, K., Harder, L. F., and Chung, R. M., 1984. *The Influence of SPT Procedures in Soil Liquefaction Resistance Evaluations*, UCB/EERC-84/15, Earthquake Engineering Research Center, University of California, Berkeley, CA.

Sowers, G. F., and Hedges, C. S., 1966. Dynamic cone for shallow in-situ penetration testing, *Vane Shear and Cone Penetration Resistance Testing of In-Situ Soils*, ASTM STP 399, American Society for Testing and Materials, 29–37.

Taboada-Urtuzuastegui, V., and Dobry, R., 1998. Centrifuge modeling of earthquake-induced lateral spreading in sand, *Journal of Geotechnical and Geoenvironmental Engineering*, ASCE, **124**,1195–1206.

Nicholson, P. G., 2006. Liquefaction evaluation discrepancies in tropical lagoon soils, *Geotechnical and Geological Engineering* **24**, 1259–1269.

Wells, D., 2010. Personal communication.

Werner, S. D., McCullough, N., Bruin, W., Augustine, A., Rix, G., Crowder, B., and Tomblin, J., 2011. Seismic performance of Port de Port au Prince during the Haiti Earthquake and post-earthquake restoration of cargo throughput, *Earthquake Spectra* **27**, this issue.

Whitman, R. V., 1971. Resistance of soil to liquefaction and settlement, *Soils and Foundations* **11**, 59–68.

Youd, T. L., Hansen, C. B., and Bartlett, S. F., 2002. Revised multilinear regression equations for prediction of lateral spread displacement, *Journal of Geotechnical and Geoenvironmental Engineering*, ASCE, **128**, 1007–1017.

Youd, T. L., Idriss, I. M., Andrus, R. D., Arango, I., Castro, G., Christian, J. T., Dobry, R., Finn, W. D. L., Harder, L. F., Hynes, M. E., Ishihara, K., Koester, J. P., Liao, S. S. C., Marcuson, W. F., Martin, G. R., Mitchell, J. K., Moriwaki, Y., Power, M. S., Robertson, P. K., Seed, R. B., and Stokoe, K. H., 2008. Liquefaction resistance of soils—Summary report from the 1996 NCEER and 1998 NCEER/NSF workshops on evaluation of liquefaction resistance of soils, *Journal of Geotechnical and Geoenvironmental Engineering*, ASCE, **127**, 297–313.

Zhang, G., Robertson, P. K., and Brachman, R. W. I., 2008. Estimating liquefaction-induced lateral displacements using the standard penetration test or cone penetration test, *Journal of Geotechnical and Geoenvironmental Engineering*, ASCE, **130**, 861–871.

(Received 6 October 2010; accepted 23 July 2011)